https://doi.org/10.3311/PPee.21747

Periodica Polytechnica Electrical Engineering and Computer Science, 68(2), pp. 178–192, 2024

Geometric Parameter Optimization of Switched Reluctance Machines for Renewable Energy Applications using Finite Element Analysis

Imed Mahmoud[1,3*], Adel Khedher[2,3]

[1] Department of Electrical Engineering, University of Monastir, Higher Institute of Applied Science and Technology (ISSAT), Mahdia, 5000 Monastir, P.O.B. 56, Tunisia
[2] Department of Electrical Engineering, University of Sousse, National Engineering School of Sousse, Rue Khalifa Karoui Sahloul, 4054 Sousse, Tunisia
[3] Laboratory of Advanced Technology and Intelligent Systems (LATIS), 4023 Sousse, P.O.B. 264, Tunisia
[*] Corresponding author, e-mail: mahmoud.imed@issatm.rnu.tn

Received: 24 December 2022, Accepted: 20 September 2023, Published online: 03 January 2024

Abstract

The choice of SRM design depends on the specific application and performance requirements. Factors such as power output, torque characteristics, and efficiency will all influence the choice of SRM design. To find an optimal geometry, it is therefore necessary to determine the effect of each parameter such as rotor pole angle, stator pole angle, stator external diameter, rotor diameter, air gap length, rotor yoke, stator yoke and shaft diameter on the machine performance. For this reason, this paper discusses a comparative study of the geometric parameters influence on SRM performance. The analysis is performed by finite element simulations based on the variation of rotor inclination, air gap length, stator and rotor pole arc variations of three machine topologies such as the three-phase 12/8 SRM, three-phase 6/4 SRM and four-phase 8/6 SRM. For a reasonable comparison, these machines must have the same basic dimensions (stator outer diameter, rotor outer diameter and length) and operate in the same magnetic circuit saturation. Graphical and numerical results of torque and magnetic flux of the three SRM topologies are highlighted. The presented study aims to provide reliable results on the dimensions to be adjusted for various applications.

Keywords

switched reluctance machine, effect analysis, finite element analysis, average torque, sensitivity analysis, torque ripple

1 Introduction

In industrial applications, the switched reluctance machine (SRM) has gained much interest. It is a good candidate for electric or hybrid vehicles, [1–3], electrical energy production, [4–6], in aeronautics, [7, 8], and flywheel energy storage system, [9]. SRM has several advantages, such as robust construction without windings or magnets on the rotor, high reliability, low manufacturing cost, high torque, insensitivity to high temperatures, and fault tolerance, [10–14]. Its main disadvantages are the discontinuous torque and the ripple effect on the torque, which cause noise and vibration, [15]. The majority of these drawbacks can be reduced by design approach, better geometry, and control methods. SRMs differ structurally and in terms of performance from traditional electric machines. SRM is a doubly salient electrical machine that cannot operate without power electronic switches.

The SRM performance is heavily dependent on its design and control, which allows for minimized torque ripple and improved torque characteristics [16]. Over the years, few authors have discussed the problem of SRM performance sensitivity in relation to its dimensions. Thus, the SRM project is a challenge for a designer to choosing the values of particular dimensions of the proper design methodology. Authors in, [17] compares mechanical vibration between a double-Stator SRM and a conventional SRM. An electromagnetic finite-element (FEA) method is used to compute acceleration, deformation, and velocity of the vibrating surface at selected point on the outer surface of the machine. In [18], the authors studied the influence of geometric parameters using the FEA for two motor topologies such as, a three-phase 6/4 SRM and a four-phase 8/6 SRM. In [19] the authors investigated how to mitigate the torque

Cite this article as: Mahmoud, I., Khedher, A. "Geometric Parameter Optimization of Switched Reluctance Machines for Renewable Energy Applications using Finite Element Analysis", Periodica Polytechnica Electrical Engineering and Computer Science, 68(2), pp. 178–192, 2024. https://doi.org/10.3311/PPee.21747

ripple through the variation of SRM geometrics parameters based on finite element simulation results. In [20] a parametric electromagnetic model is developed for the switched reluctance generator (SRG) with FEA which can be considered appropriately for accurate analysis and optimal design of the SRG. Innovations on design of 6 × 4 and 6 × 6 SRG is presented to increase the efficiency in [21].

The sensitivity analysis is an important study for any motor designer, [19, 22]. Several design and geometrical parameters affect the electrical drives performance differently. In a design of a SRM, to find an optimum geometry, it is important to analyze how each parameter impacts the machine's performance. Consequently, the designer has to look for solutions that are feasible for all performance parameters. However, we are concentrated on parametric sensitivity analysis to determine the influence of the main parameters in the average torque and torque ripple. The main objective of this article is to analyze the influence of geometric parameters on the performance of three different SRM topologies: the three-phase 12/8 SRM, three-phase 6/4 SRM, and four-phase 8/6 SRM. The specific objectives are as follows:

- Determine the effect of rotor pole angle, stator pole angle, stator external diameter, rotor diameter, air gap length, rotor yoke, stator yoke, and shaft diameter on the performance of SRMs.
- Conduct a comparative study of the torque and magnetic flux characteristics of the three SRM topologies under different geometric parameter variations.
- Develop a computer program using Magnet-2D for finite element simulations to accurately analyze the magnetic behavior and performance of the SRM topologies.
- Provide reliable insights and numerical results on the dimensions that need to be adjusted for optimizing the performance of SRMs in renewable energy applications.

This paper is organized as follows. Taking apart the introduction and the conclusion, in Section 2 the pre-sizing of the SRM is presented. Section 3 presents the finite elements analysis (FEA) of the three motors. The influence analysis of the geometrical parameters variation results are presented in Section 4.

2 Pre-sizing of the switched reluctance machine

Over the years, research has been based mainly on the design of an electric machine. The SRM design is apparently similar to traditional machine design but differs in several points due to SRM's unique features. Some characteristics simplify the design, such as the absence of coils and magnet in the rotor, ability to operate over a wide speed range and absence of brushes. Nevertheless, other characteristics such as inductance nonlinearity, excessive saturation for some rotor positions and the complexity of modeling SRM make this a complex process.

The SRM performance analysis, both electric and magnetic, depends on its geometry, construction and materials used, [23]. It is almost impossible to determine exact mathematical equations that take into account all these influential parameters [23]. In this way, the main idea of this work is to develop a model that incorporates the some parameters independently. Also, it is able to give useful results to calculate the electric machine performance. Fig. 1 illustrates all the dimensions that must be determined for the construction of an SRM, where g is the length of the air gap, D_s is the outer diameter, D_r is the inner diameter, D_0 is the shaft diameter, β_r is the rotor pole arc, β_s is the stator pole arc, H_s is the stator pole height, H_r is the rotor pole height, Y_s is the stator back iron thickness, and Y_r is the rotor back iron thickness.

To avoid the appearance of parasitic currents caused by the magnetic flux dispersion effect. It is must meet the following constructive relations:

$$\beta_r \geq \beta_s, \quad (1)$$

$$\beta_s + \beta_r \leq \frac{2\pi}{N_r}. \quad (2)$$

To reduce the torque ripple, a third constructive relation must be followed. The angular distance between adjacent phase inductance (ε) is defined by Eq (3):

$$\varepsilon = \frac{2\pi}{\frac{N_s}{2} \times N_r}. \quad (3)$$

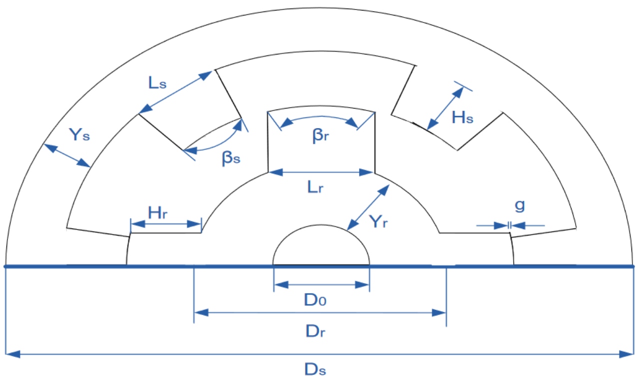

Fig. 1 Switched reluctance machine (SRM) dimensions

The minimum value for stator polar arcs is determined from the machine poles number by Eq. (4).

$$\min(\beta_s) = \frac{4\pi}{N_s \times N_r}. \quad (4)$$

The conditions presented in Eqs. (1)–(4) can be represented graphically in a triangle of possibilities. It is necessary that the values of the polar arcs of the machine are in this triangle. Fig. 2 shows the possibility triangle for a 12/8 SRM, an 8/6 SRM and a 6/4 SRM, [24].

The conditions for the choice of stator and rotor pole angles can be represented graphically in a possibility triangle. The values of the polar arcs of the machine need to be within this triangle [25].

The SRM power output equation is presented by [26]. From this equation, we determined the inner diameter of SRM.

$$D_r = \sqrt[3]{\frac{P}{B \times n \times K_1 \times K_2 \times a_s \times K \times K_E \times K_D}} \quad (5)$$

With B is the flux density, a_s the specific electric loading, K the relationship with the core length, K_1 constant, K_2 the ratio between the inductance values in the unaligned and aligned position, K_E the efficiency, K_D the duty cycle, n the rotor speed in rpm and P is the power.

The core length is demonstrated as a multiple of the inner diameter D_r, as given by Eq. (6). The value of K is decided by the motor application nature. Equations (7) and (8) gives respectively the interval of K for servo and non-servo applications:

$$L = K \times D_r, \quad (6)$$

$$0.25 \le K \le 0.7, \quad (7)$$

$$1 \le K \le 3. \quad (8)$$

Moreover, the outer diameter D_s is determined as a multiple of the inner diameter. This relationship is depicted in Eq. (9):

$$D_s = \frac{D_r}{C_{D_s}}. \quad (9)$$

With C_{D_s} is internal diameter:

$$0.4 \le C_{D_s} \le 0.7. \quad (10)$$

The air gap length has an effective influence on magneto motive force produced by the magnetic circuit. For SRM, the air gap must be as small as possible to achieve a high average torque. For this reason, its value should be chosen according to the machine size. For the machine with power less than 1 kW, the air gap should range between 0.18 and 0.25 mm, [26]. Moreover, for the machines with power above 1 kW may have air gaps from 0.3 to 0.5 mm [26].

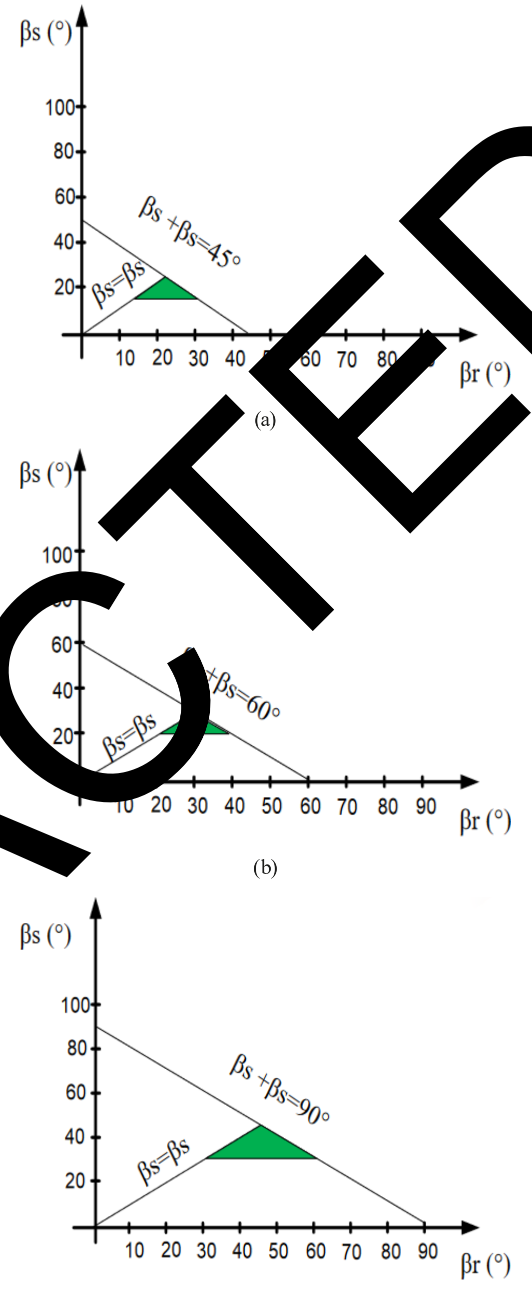

Fig. 2 Limits of the pole arcs; (a) 12/8 SRM three-phase, (b) 8/6 SRM four-phase and (c) 6/4 SRM three-phase

The stator width L_s and rotor width L_r poles are given by Eqs. (11) and (12) [27]:

$$L_s = D_r \times \sin\left(\beta_s/2\right), \quad (11)$$

$$L_r = \left(D_r - 2\times g\right)\times \sin\left(\beta_r \big/ 2\right). \quad (12)$$

However, to improve robustness and minimize vibration and noise, an additional factor should be considered. Consequently, the value of the stator and rotor yokes thickness should be in the range:

$$L_s > Y_s \geq 0.5\ L_s, \quad (13)$$

$$0.5\ L_r < Y_r < 0.75\ L_r. \quad (14)$$

To calculate the stator and rotor poles height value, you need the outer and inner diameter values as well as the stator yoke thickness. There expressions are shown respectively in Eq. (15) and (16):

$$H_s = \frac{D_s - D_r - 2\ Y_s}{2}, \quad (15)$$

$$H_r = \frac{D_s - D_0 - 2\ g - 2\ Y_r}{2}. \quad (16)$$

The turn's number per phase can be obtained from Eq. (17) for a given maximum current on the conductor [28]:

$$n = \frac{2\ g}{I_{peak}}\times H. \quad (17)$$

3 Finite elements analysis

In order to characterize the magnetic behavior over the entire field of the three motors topologies, a computer program was developed with the help of finite element methods. The first model is built according to the reference motor with a topology 8/6 [29]. The rated power is 2.2 kW and the rated current is 10 A. Under these conditions, the second and third model has the same dimensions, but different in the number of stator and rotor poles (topology 12/8 and 6/4). Some significant mechanical parameters of the three topologies are shown in Table 1.

An understanding of the SRM requires a detailed analysis of torque and inductances for different positions of the rotor and at different values of stator excitation currents. In order to characterize the magnetic behavior over the entire field of the machine under study, a computer program was developed with the help of finite element methods. This program has allowed us to obtain databases illustrated in Figs. 3–5. These databases are presented in the form of three-dimensional graphs, showing the relationships between torques, inductances and currents, also the magnetic field distribution respectively for the three topologies such as 12/8 SRM, 8/6 SRM and 6/4 SRM.

Table 1 Motors mechanical parameters

Parameters	Unit	8/6 SRM	12/8 SRM	6/4 SRM
Rotor pole angle	β_r	24.5°	17°	32°
Stator pole angle	β_s	22.5°	15°	[illegible]
Stator external diameter	D_s	160 mm	160 mm	160 mm
Rotor diameter	D_r	91.1 mm	[illegible] mm	91.1 mm
Air gap length	g	0.3 mm	0.3 mm	0.3 mm
Stator pole height	H_r	13 mm	13 mm	13 mm
Rotor pole height	H_s	[illegible] mm	22 mm	[illegible] mm
Rotor yoke	Y_s	12.45 mm	12.45 mm	12.45 mm
Stator yoke	Y_r	15 mm	15 mm	15 mm
Shaft diameter	D_0	34.5 mm	34.5 mm	34.5 mm

4 Influence analysis of the geometric parameters variation

To improve torque characteristics such as reducing torque ripples and increasing average torque, the SRM geometry needs to be modified. In order to investigate the influence of different SRM geometries on electromagnetic torque, the following parameters will be modified: air gap length g, skewed rotor teeth, rotor and stator pole arc.

4.1 Influence of air gap variation

If we assume that the leaks are negligible, the iron reluctance on a pole pitch is assumed to be zero. Consequently, taking into account this simplifying assumption, the reluctance will be reduced to that of the air gap described by this expression:

$$\Re = \frac{g}{\mu S}. \quad (18)$$

In order to make a more precise influence analysis of this parameter on the behavior of SRM, we considered a series of numerical simulations by the FEA corresponding to a variable air gap. Fig. 6 gathers the results obtained and compares them for the three topologies of SRM

Fig. 6 shows the sensitivity of the maximum torque generated by the machine as a function of the air gap. The latter is therefore a significant factor to be taken into consideration. It therefore seems necessary to assign this machine a too small magnetic air gap of the order of 0.3 mm. Also, the flux linkage value increases due to the lower of magnetic flux resistance flowing from stator to rotor. Hence, the torque value in the aligned position to the unaligned position also increases.

It clearly shows the strong influence on the maximum torque as well as the flat torque range on the characteristics for different topologies. Hence, the machine with the smallest air gap length will produce the highest average

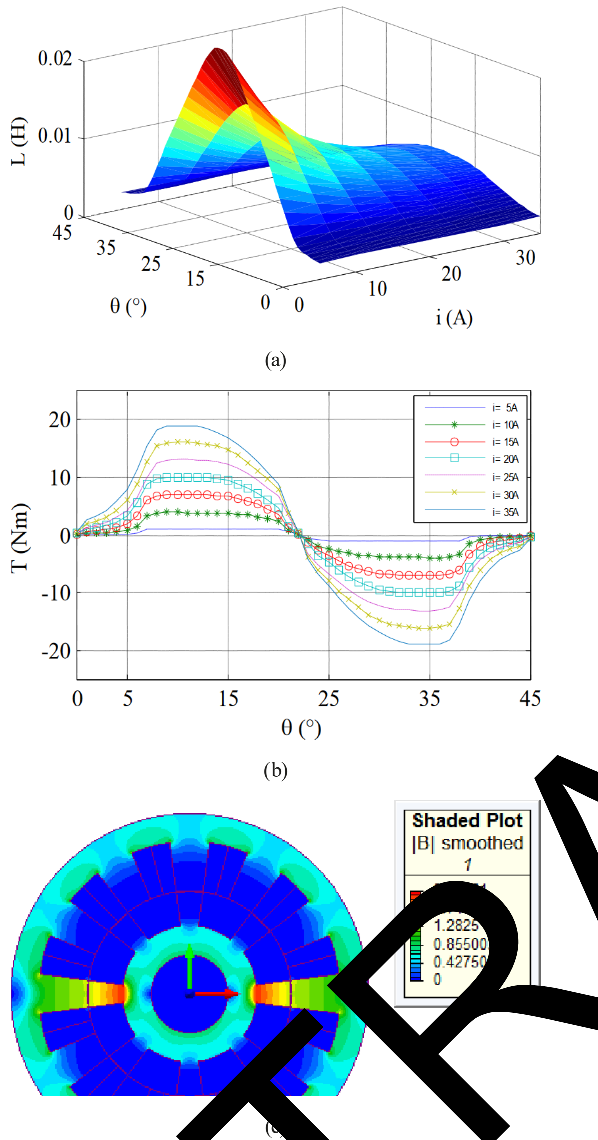

Fig. 3 12/8 SRM topology; (a) inductance profile; (b) torque profile and (c) magnetic field distribution for i = 10 A

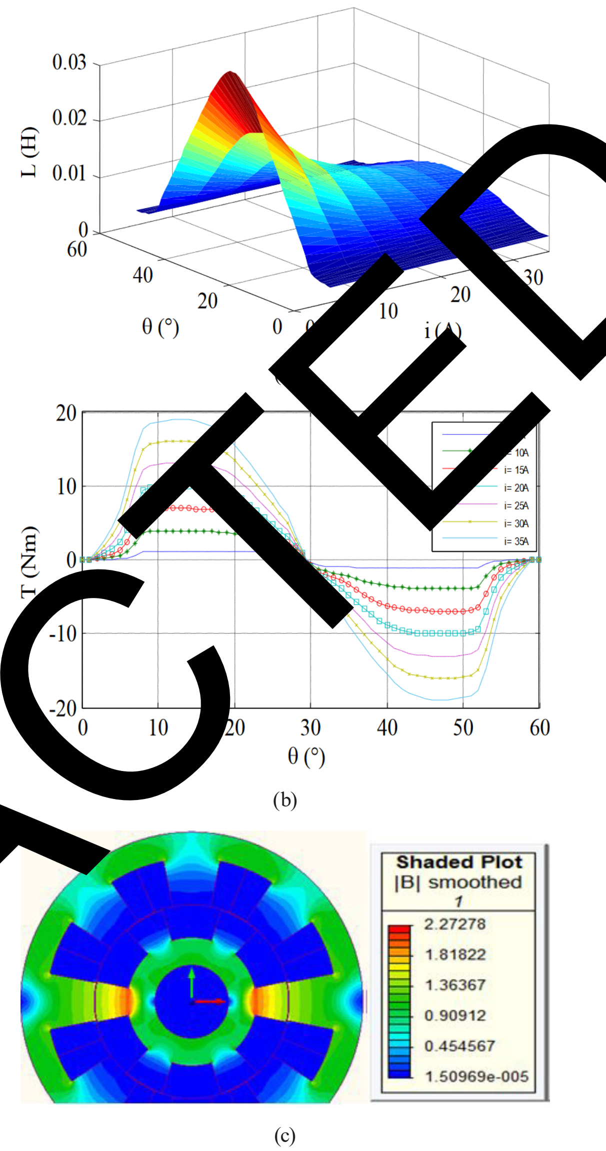

Fig. 4 8/6 SRM topology; (a) inductance profile, (b) torque profile and (c) magnetic field distribution for i = 10 A

torque, as shown in Fig. 7 (a). The torque ripples referring can be slightly reduced by growing air gap length, as shown in Fig. 7 (b).

Table 2 shows the average torque and magnetic field distribution B for the air gap length variation. With an increase of 0.1 mm in air gap, the average torque value reduces about [illegible]% for SRM 12/8, 15.9% for SRM 8/6 and 18% for SRM 6/4. From the results presented of the air gap variations, it is interesting to have a lower value of the parameter g.

4.2 Influence of rotor polar arc variation

In the design step, the rotor polar arcs defined in the minimum, average and maximum values. Fig. 8 shows the defined values. The choice range of the rotor polar arcs based on the feasible triangle, Fig. 2 is:

$$\left.\begin{array}{l} 15° \le \beta_{r_{12/8}} \le 30° \\ 30° \le \beta_{r_{6/4}} \le 60° \\ 22.5° \le \beta_{r_{8/6}} \le 37.5° \end{array}\right\}. \quad (19)$$

The effect of β_r variation isillustrated by Fig. 9. We can notice this effect as well on the average torque and B values, Table 3, respectively for different topologies such as 12/8, 8/6 and 6/4 SRM.

From Fig. 9, it can be observed that the rotor pole arc has a significant influence on the shape of torque profile and on the maximum value of the flux linkage. The flux increase in the unaligned position with the increase of β_r. Furthermore, it is observed that there is no torque production when the

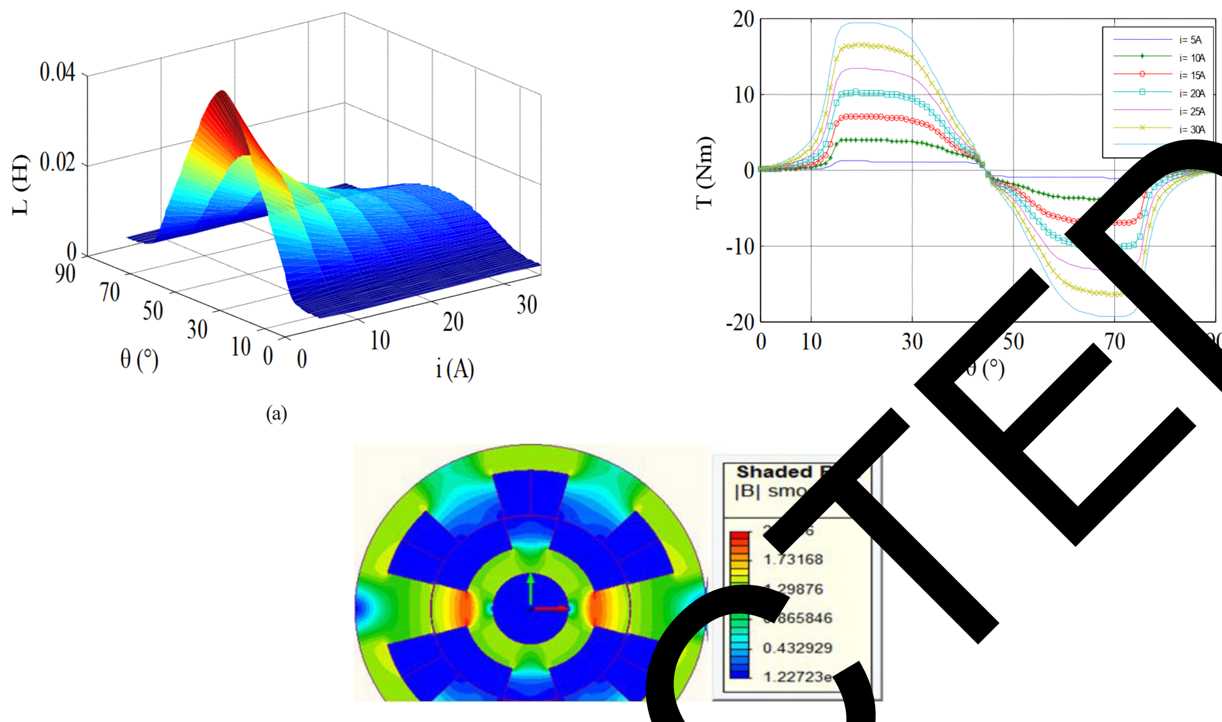

Fig. 5 6/4 SRM topology; (a) inductance profile, (b) torque profile and (c) magnetic field distribution for i = 10 A

difference between β_r and β_s is very large. It causes reduction in the average torque value. For 12/8 SRM, there is no torque production when β_r = 30°. This behavior repeats for 8/6 and 6/4 SRM when β_r = 37.5° and β_r = 60° respectively, as are the values presented in Table 3.

4.3 Influence of stator polar arc variation

The range for choosing the polar arc of the stator is determined by the possibilities triangle displayed in Fig. 2. Eq. (20) presented the stator polar arc range:

$$\left.\begin{array}{l} 7.5° \le \beta_{s_{12/8}} \le 22.5° \\ 30° \le \beta_{s_{6/4}} \le 45° \\ 15° \le \beta_{r_{8/6}} \le 30° \end{array}\right\}. \quad (20)$$

Fig. 10 illustrates the flux linkage and torque plots for different topology of SRM. Table 4 provides results of the average torque and B for each SRM.

It is apparent from Fig. 10 that the value of β_s has an effectively influence on the flux linkage and torque in the machines studied. The increase of the stator polar arc induces an increase on the flux value in the unaligned position, due to the larger overlap area with the rotor pole. Furthermore, the larger β_s value gives a longer duration of torque production. Consequently, there is a significant change in the shape of the torque profile for three motors. Through from Table 4, it is observed that the increase of β_s gives growth of average torque and B values. Thus, the choice of the stator polar arc value must take into account the space between poles, to accommodate the coils.

4.4 Influence of skewed teeth shapes

The effect of skewing the stator, rotor, or both structures in order to reduce vibration and acoustic noise in SRMs is evaluated in this section. Fig. 11 illustrate the definition of the skewing angle for the stator and the rotor teeth. The skewing angle is the difference in angular position between the upper and the bottom corners of the pole measured from the stator center. The same definition applies to the rotor's skewing angle.

Three motors with different skewing techniques (skewed-stator, skewed-rotor, and both skewed) are designed for the three topologies such as 8/6 SRM, 6/4 SRM and 12/8 SRM, as shown in the Fig. 12. The three motors keep the same basic dimension in Table 1 but with different skewing angels. The range for choosing the skewing angels is present in Eq. (21) [29]. We choose the same skewing angels for the three topologies.

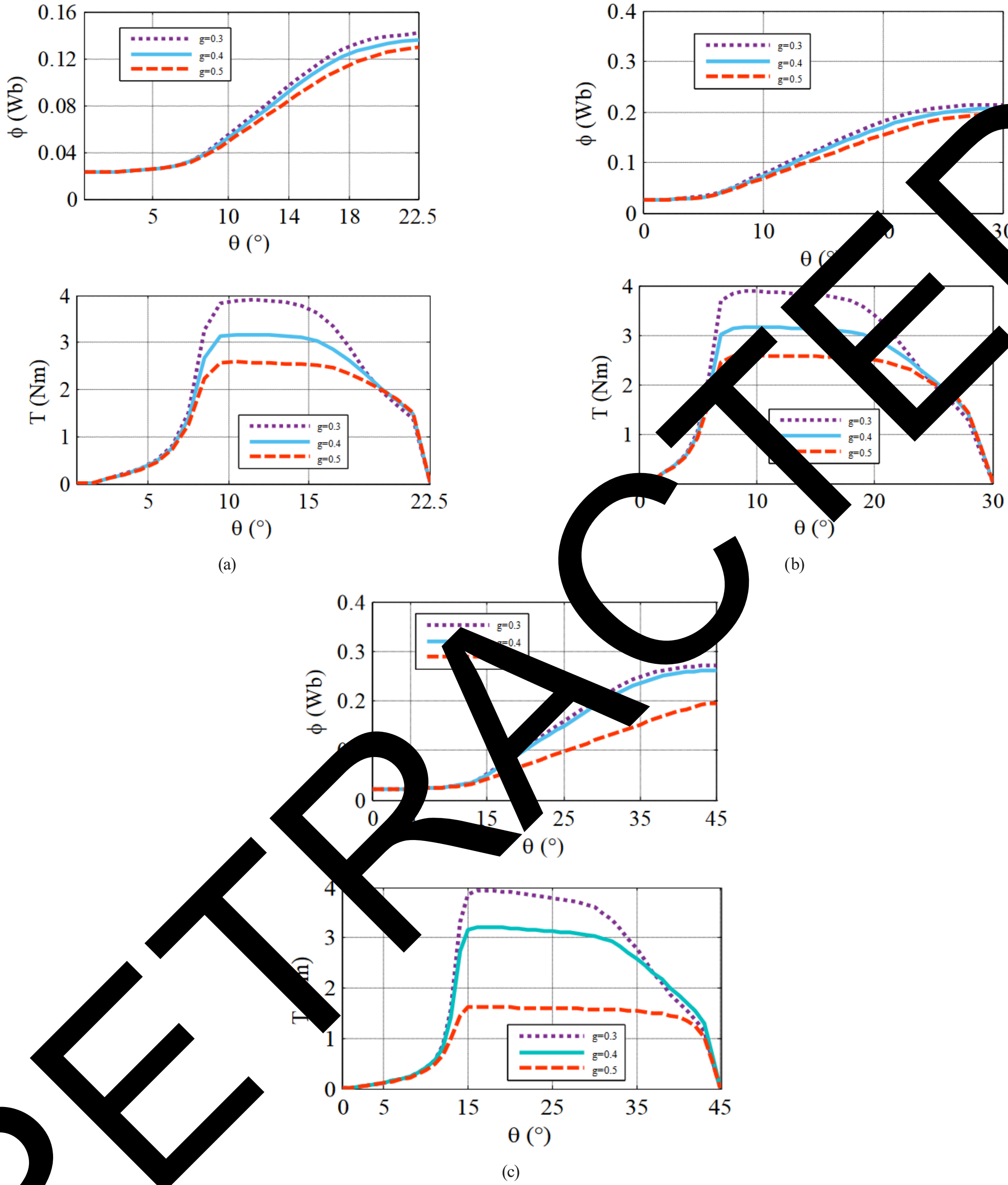

Fig. 6 Influence of air gap (g) variation on torque and flux linkage; (a) SRM 12/8; (b) SRM 8/6 and (c) SRM 6/4

$$\theta_s = \frac{360}{N_s} \quad (21)$$

The RS-SRM is composed by assembling the normal stator and rotor skewed, the SS-SRM is obtained by assembling the stator skewed and normal rotor, and the RSS-SRM is composed by assembling the rotor and the stator skewed.

Figs. 13 and 14 shows comparisons of the static flux linkage and torque between the conventional SRM, RS-SRM, SS-SRM, and RSS-SRM, in the case of 20° skewing angle. In Fig. 13, compared to the conventional SRM, the torques increases slightly, as shown in Table 5. However, the rises of torque will result an increase in performance. As shown in the figure, the torque phases of the SS-SRM and RS-SRM are lagged for 18° and

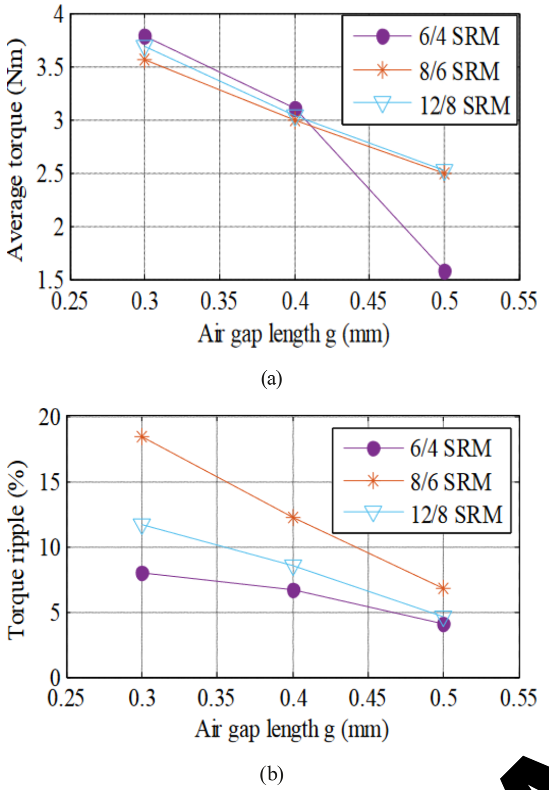

Fig. 7 Effect of air gap length on; (a) average torque; (b) torque [illegible]ple

Table 2 Results of air gap (g) variation

Type of motor	Variable	Average tor[illegible]	B ([illegible]
	$g = 0.3$	[illegible]589	2.056
SRM 12/8	$g = 0.4$	3.041	2.013
	$g = 0.5$	[illegible]525	[illegible]
	$g = 0.3$	3[illegible]	2.056
SRM 8/6	$g =$ [illegible]	2.989	2.019
	[illegible]0.5	2.499	1.999
	$g = 0.3$	3.788	2.101
SRM 6/4	$g = 0.4$	[illegible]107	1.858
	g [illegible]0.5	[illegible]582	1.565

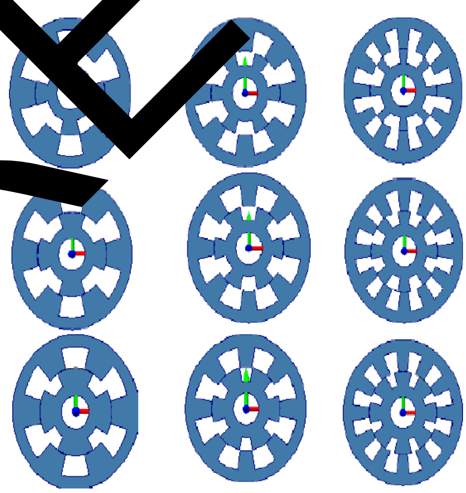

Fig. 8 Different SRM geometry for minimum, average and maximum rotor polar arcs values respectively

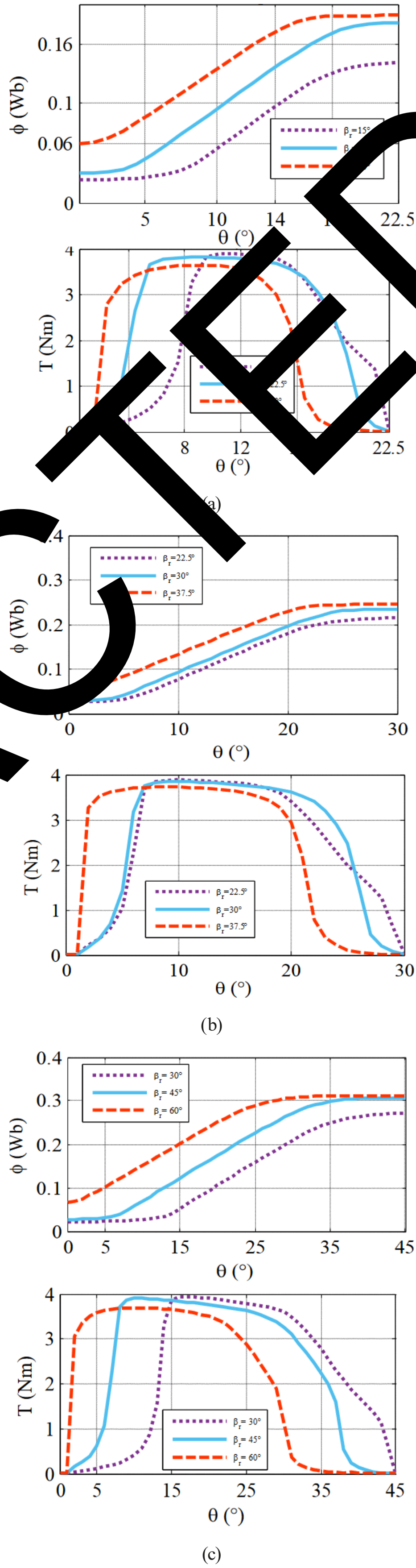

Fig. 9 Influence of rotor polar arc (β_r) variation on flux linkage and torque; (a) SRM 12/8, (b) SRM 8/6 and (c) SRM 6/4

Table 3 Results of rotor polar arc (β_r) variation

Type of motor	Variable	Average torque (N m)	Torque ripple (%)	***B*** (*T*)
	$\beta_r = 15°$	3.831	9.55	1.828
SRM 12/8	$\beta_r = 22.5°$	3.781	2.43	1.782
	$\beta_r = 30°$	3.566	3.70	1.725
	$\beta_r = 22.5°$	3.435	25.90	1.898
SRM 8/6	$\beta_r = 30°$	3.561	11.40	1.864
	$\beta_r = 37.5°$	3.503	7.85	1.832
	$\beta_r = 30°$	3.812	7.18	1.939
SRM 6/4	$\beta_r = 45°$	3.795	6.53	1.846
	$\beta_r = 60°$	3.614	4.53	1.610

advanced for 18°, respectively for 6/4 SRM and 8/6 SRM. In Fig. 13 (c), the torque of RSS-SRM compared with the traditional one advanced for 2.

As appeared in Fig. 14, the flux linkage profile of the RS-SRM and SS-SRM changes more significantly than the conventional SRM. Moreover, the flux linkages for the different topologies have a perfect match of RSS-SRM with the traditional one. The flux phases of the SS-SRM [illegible] RS-SRM are a leading 20° and a lagging 20°, respecti[illegible]ly for 6/4 SRM and 8/6 SRM, as shown in Fig. 14 (a) and ([illegible] For 12/8, SRM the flux phases of the RS-SRM is leadin[illegible] for 15°, as shown in Fig. 14 (c). Compare[illegible] conven-tional SRM, saturation increases wit[illegible]ifferent t[illegible] angles for both the 6/4 SRM and 8/6 SR[illegible]opologie[illegible]hown in Table 5. Conversely, saturati[illegible] decr[illegible]es [illegible]th tilt angles for 12/8 SRM.

The electromagneti[illegible]teristic of the [illegible]M can be determined by the s[illegible]c torqu[illegible] different curr[illegible]nt ranges and rotor positi[illegible]s. The electro[illegible]gnetic characteristic curves of th[illegible]SS-SRM presented a[illegible]he static torque is shown in [illegible]. 15.

4.5 Radial [illegible]nalysis

[illegible]aper t[illegible]lculat[illegible]e air gap forces, we will use the Ma[illegible]ell stress [illegible]. The stress tensor T is presented as [29[illegible]

$$[illegible] = \frac{1}{\mu_0}\left[\left(B\times\hat{\boldsymbol{n}}\right)B-\frac{1}{2}\left(\nabla B^2\hat{\boldsymbol{n}}\right)\right]. \quad (22)$$

where [illegible] is the unit normal vector, μ_0 is the permeability of free space and B is flux density. The derivation of the mathematical model of the force is based on the Maxwell stress tensor. According to the method of Maxwell stress, the total force is given as follows [29, 30]:

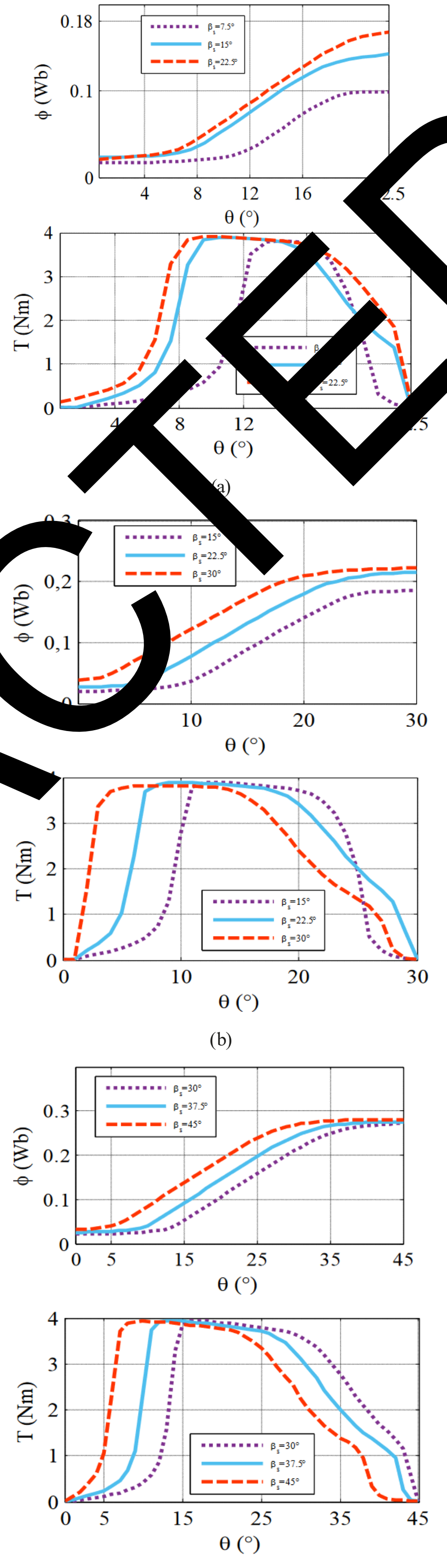

Fig. 10 Influence of stator polar arc (β_s) variation on flux linkage and torque; (a) SRM6/4; (b) SRM 8/6 and (c) SRM 12/8

Table 4 Results of stator polar arc (β_s) variation

Type of motor	Variable	Average torque (N m)	Torque ripple (%)	***B*** (*T*)
	$\beta_s = 7.5°$	3.095	47.04	1.740
SRM 12/8	$\beta_s = 15°$	3.685	12.13	1.828
	$\beta_s = 22.5°$	3.835	0.91	1.918
	$\beta_s = 15°$	3.342	33.66	1.876
SRM 8/6	$\beta_s = 22.5°$	3.553	18.40	1.898
	$\beta_s = 30°$	3.565	14.33	1.974
	$\beta_s = 30°$	3.782	8.19	1.890
SRM 6/4	$\beta_s = 37.5°$	3.762	6.93	1.895
	$\beta_s = 45°$	3.794	7.24	1.939

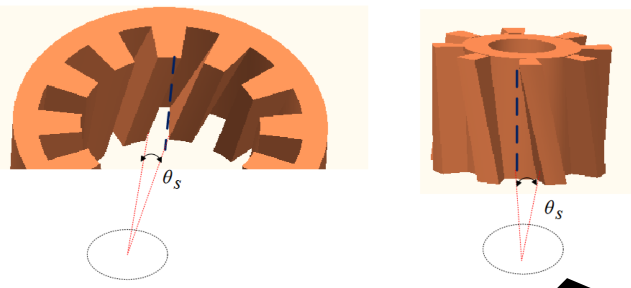

Fig. 11 Definition of the skewing angle

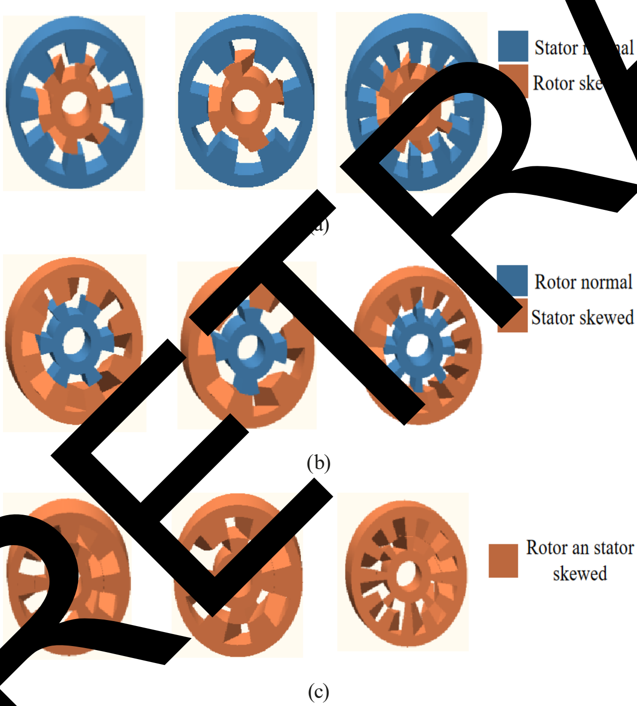

12 The SRM structures; (a) RS-SRM; (b) SS-SRM and (c) RSS-SRM

$$f = \int T \ ds. \tag{23}$$

The electromagnetic force f can be divided into tangential and radial components. The tangential force f_T and the radial force f_R acting on an integral surface can be described as follows:

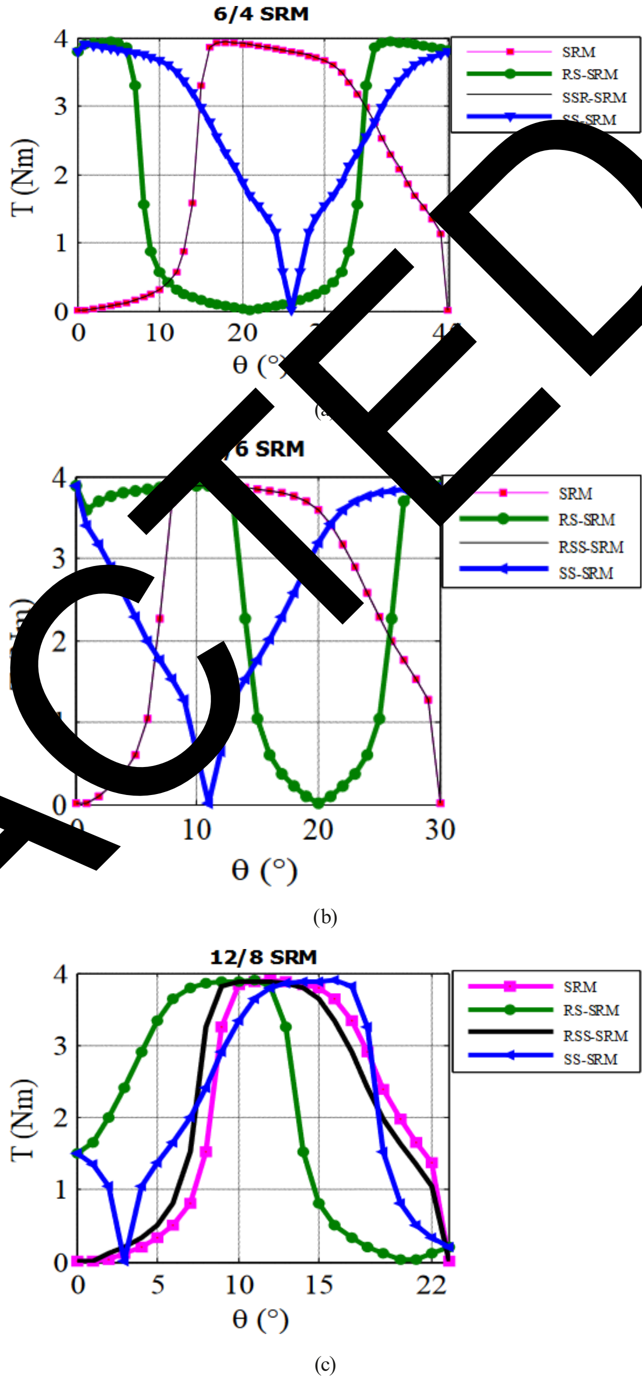

Fig. 13 Torque profile for the SRM, RS-SRM, SS-SRM, and RSS-SRM; (a) 6/4 SRM; (b) 8/6 SRM and (c) 12/8 SRM at 10 A

$$f_T = \frac{1}{\mu_0} \iint B_T \times B_R \ ds, \tag{24}$$

$$f_R = \frac{1}{2\mu_0} \iint \left(B_R^2 - B_T^2 \right) \ ds, \tag{25}$$

where B_T and B_R are the tangential and radial magnetic component of the flux density from the tangential direction and vertical direction, respectively. The radial force is the major cause of acoustic noise and vibration in SRMs.

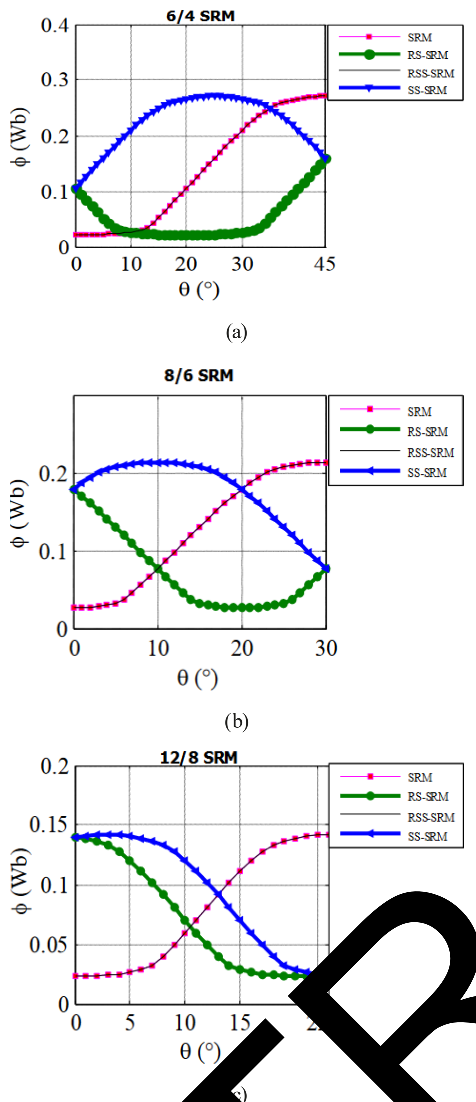

Fig. 14 Flux linkage for [illegible] SRM, [illegible]RM, SS-SRM, an[illegible]SS-SRM; (a) 6/4 SRM[illegible] (b) 8/6 SRM and [illegible]2/8 SRM at 10 A

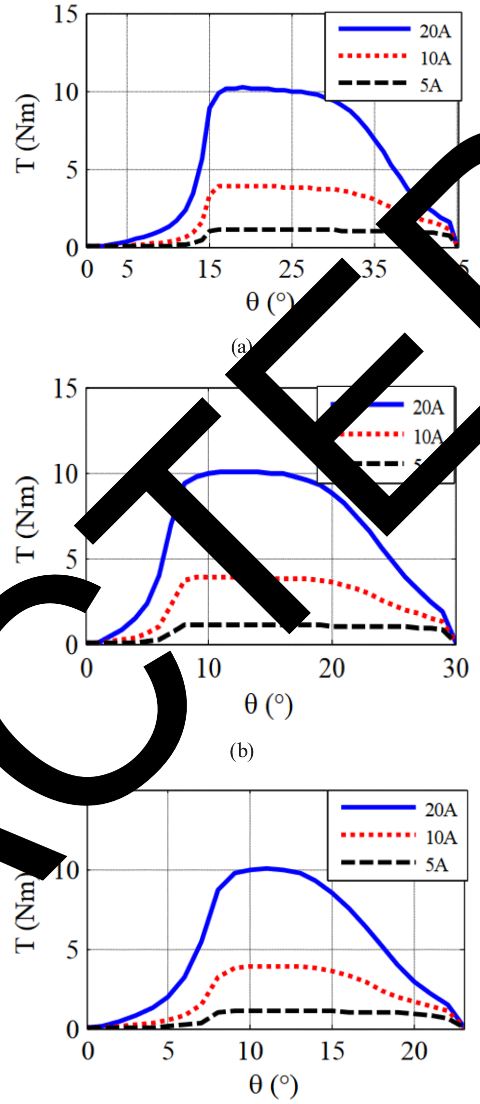

Fig. 15 RSS-SRM torque profile for different current; (a) 6/4 SRM; (b) 8/6 SRM and (c) 12/8 SRM

[illegible]**able 5** Results of skewed teet[illegible]apes

Type of [illegible]r	Vari[illegible]e	Average torque (N m)	B (T)
[illegible]	[illegible]RM	3.68	1.56
	[illegible]SS-SRM	3.89	1.48
	[illegible]SR[illegible]	3.90	0.27
	SS-[illegible]M	3.88	0.158
[illegible]6 SRM	[illegible]SRM	3.86	1.51
	RSS-SRM	3.85	1.55
	RS-SRM	3.93	2.14
	SS-SRM	3.88	2.39
6/4 SRM	SRM	3.78	1.51
	RSS-SRM	3.94	1.51
	RS-SRM	3.93	1.96
	SS-SRM	3.90	2.05

The radial force at the stator structure can be determined by an FEA method using Eq. (25), where the integration surface is the end of the stator poles.

Figs. 16, 17 and 18 shows the comparisons of the radial force in RS-SRM, SS-SRM, and RSS-SRM, respectively with different skewing angles for the three topologies. The skew angles of the motors are chosen at 5°, 10°, 15° and 20° respectively for this study. The motors are simulated in the same operations, at the rotor alignment position of phase A with a phase current of 10A.

The maximum radial force of the SR-SRM, SS-SRM and RSS-SRM are all reduced when the skewed angle increases from 5° to 20° for the three topologies 6/4 SRM, 8/6 SRM and 12/8 SRM.As shown in Fig. 16, when the rotor is skewed with different angles, the radial force varies with respect to different variation. Compared to RS-SRM 6/4 and RS-SRM 12/8, the peak of radial force distributed on the stator yoke are much smaller for RS-SRM 8/6, as shown in Fig. 16(b), which can reduce stator vibration and deformation. Fig. 17 shows the skewing angle for the SS-SRM. The radial force is also reduced at 20° and more lower for the SS-SRM 8/6, which is similar to the force distribution in the RSS-SRM, as shown in Fig. 18. Based on the above analysis, the acoustic noise level and vibration are directly related to stator deformation and the poles numbers of SRM.

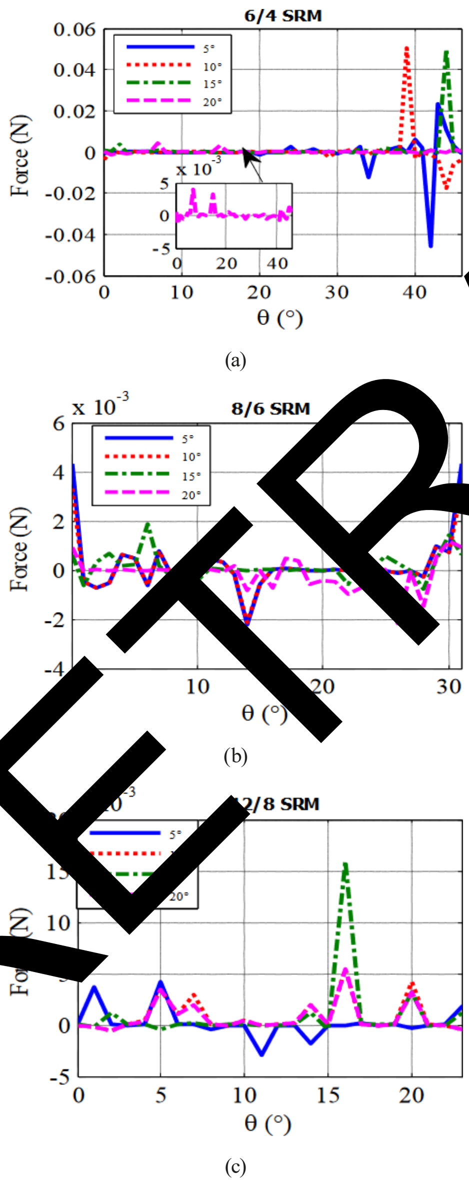

Fig. 16 Radial force variation for RS-SRM with different skewing angles; (a) 6/4 SRM; (b) 8/6 SRM and (c) 12/8 SRM

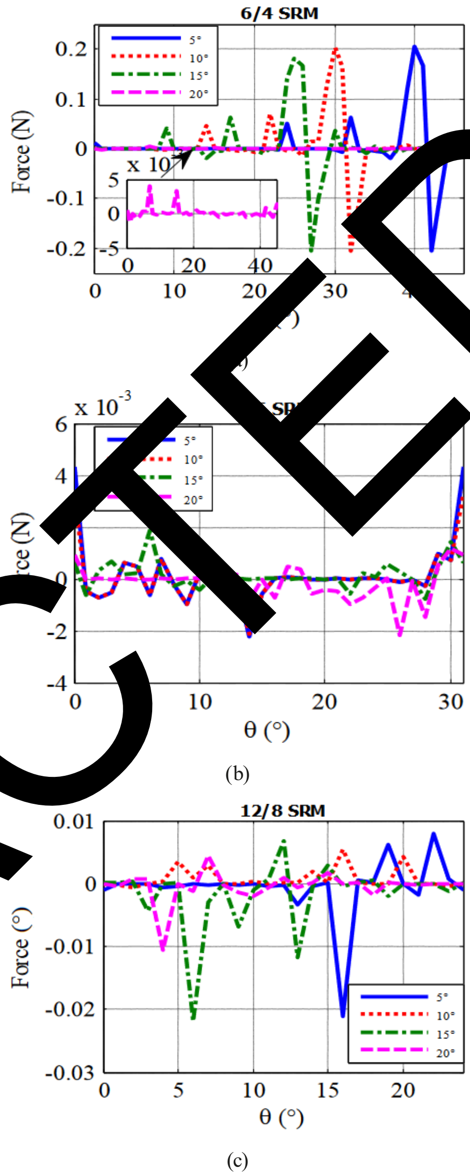

Fig. 17 Radial force variation for SS-SRM with different skewing angles; (a) 6/4 SRM; (b) 8/6 SRM and (c) 12/8 SRM

5 Conclusion

This paper presented a quantitative comparison between three doubly salient switched reluctance motors under equal conditions. The SRM design procedures are presented. We highlighted the dimensions influence on the SRM performance through finite element analysis (FEA) of a 12/8 three-phase SRM, a 6/4 three-phase SRM, and an 8/6 four-phase SRM. The SRM electromagnetic behaviors such as torque and flux characteristics are illustrated to show the performance of the three motors topologies. The impact of four dimensions on the average torque value and torque ripple was analyzed, the experiments were conducted through FEA. From this work, it is found that:

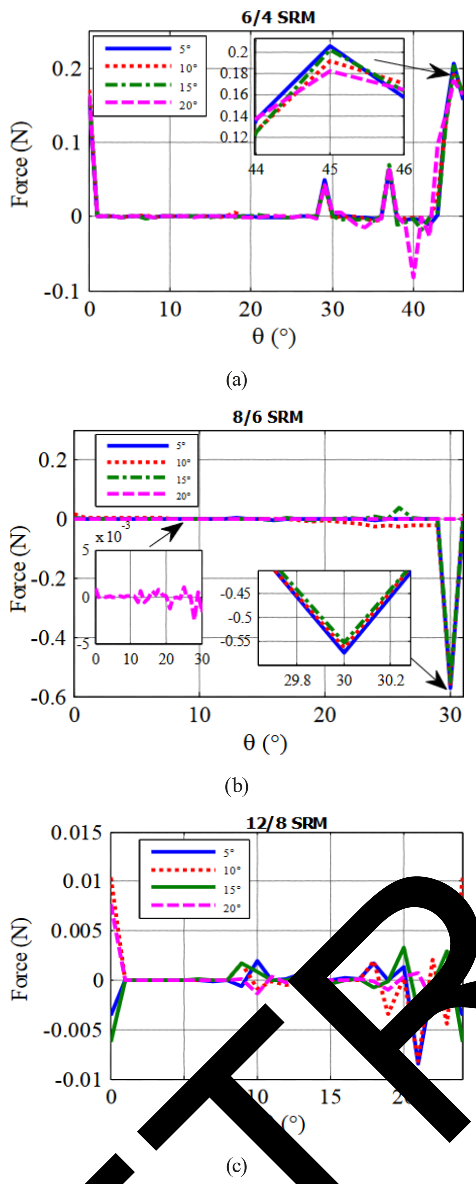

Fig. 18 Radial force variation for RSS-SRM with different skewing angles, (a) 6/4 SRM, (b) 8/6 SRM and (c) 12/8 SRM

1. The 6/4 SRM provides better performance with the minimum air gap compared with 12/8 SRM and 8/6 SRM. The torque ripple is reducing.
2. The three motors offer reduction in torque ripple and average torque with the larger angle of rotor pole arc (β_r).
3. The larger of stator pole arc (β_s) value gives a longer duration of positive torque production and minimum torque ripple, 12/8 SRM is defined by comparable reduction of the torque ripple.
4. Skewing can maximize average torque of the SRMs. 8/6 SRM and 6/4 SRM torque are all increased with the skewing angle.

6 Future work

Further investigations should explore additional SRM topologies and compare their performance with the ones studied in this analysis. This would provide a more comprehensive understanding of the influence of geometric parameters on a broader range of SRM designs.

Experimental validation of the simulation results would enhance the reliability of the findings. Conducting experimental tests on SRM prototypes with different geometric configurations would allow for a direct comparison and validation of the simulated performance characteristics.

This study primarily focuses on torque and magnetic flux characteristics. Future work could include additional performance metrics such as power density, cogging torque, and efficiency to provide a more complete evaluation of the SRM designs.

Considering the impact of practical constraints and manufacturing limitations would be valuable. Factors such as material availability, cost, and manufacturability should be taken into account to ensure the feasibility of the proposed design modifications.

Exploring advanced optimization techniques, such as genetic algorithms or machine learning algorithms, could help identify the optimal geometry for enhanced SRM performance. These techniques can consider a larger design space and provide insights into multi-objective optimization, considering conflicting performance metrics.

By addressing these limitations and pursuing future work in these directions, researchers can further enhance the understanding and design optimization of SRMs for various applications.

References

[1] Cheng, H., Wang, L., Xu, L., Ge, X., Yang S. "An Integrated Electrified Power train Topology With SRG and SRM for Plug-In Hybrid Electrical Vehicle", IEEE Transactions on Industrial Electronics, 67(10), pp. 8231–8241, 2020. https://doi.org/10.1109/TIE.2019.2947854

[2] Fathabadi, H. "Plug-in hybrid electric vehicles: Replacing internal combustion engine with clean and renewable energy based auxiliary power sources", IEEE Transactions on Power Electronics, 33(11), pp. 9611–9618, 2018. https://doi.org/10.1109/TPEL.2018.2797250

[3] Martinez, C. M., Hu, X. S., Cao, D., Velenis, E., Gao, B., Wellers M. "Energy management in plug-in hybrid electric vehicles: Recent progress and a connected vehicles perspective", IEEE Transactions on Vehicular Technology, 66(6), pp. 4534–4549, 2017. https://doi.org/10.1109/TVT.2016.2582721

[4] Bahy, M., Shanab, M. A., Nada, A. S, Elbanna, M. H. "Enhancement of high-voltage ride-through of a grid connected switched reluctance generator (SRG) wind turbine using a dynamic voltage restorer based on fuzzy logic controller", Journal of Al-Azhar University Engineering Sector, 15(55), pp. 546–559, 2020. https://doi.org/10.21608/auej.2020.87882

[5] Chen, H., Guan, G., Han, G., Chen, H. "Fault Diagnosis and Tolerant Control Strategy for Position Sensors of Switched Reluctance Starter/Generator Systems", IEEE Transactions on Trans[illegible] Electrification, 6(4), pp. 1508–1518, 2020. https://doi.org/10.1109/TTE.2020.2997349

[6] Faridnia, N., Seyedyazdi, M., Shabaninia, F. "Voltage Co[illegible] of a 12/8 Pole Switched Reluctance [illegible] Using Fu[illegible] Logic", International Journal of M[illegible]n Nonline[illegible] Theory an[illegible] Application, 1(3), pp. 107–112, 20[illegible] https://doi.org/10.4236/ijmnta.2012.[illegible]6

[7] Valdivia, V., Todd, R., Br[illegible] F. J., Bar[illegible], Lzaro, A., Forsyth, A. J. "Behavioral Mo[illegible]g of a Switche[illegible]luctance Generator for Aircraft Pow[illegible]s", IEEE Transa[illegible]s onIndustrial Electronics, 61([illegible] pp. 2690–[illegible]9, 2014. https://doi.[illegible]/10.1109/TIE.201[illegible]6768

[8] Bartolo[illegible], Degano, M., Espina, [illegible] Gerada, C. "Design and Initi[illegible]esting of a High-Speed 45-kW [illegible]witched Reluctance Drive f[illegible] Aerospace [illegible]plication", IEEE Transactions on Industrial El[illegible]nics, [illegible]), pp. 988–9[illegible]7, 2014. https://[illegible]g/10.1109/TI[illegible]16.2618342

[9] [illegible]ardenas, [illegible] Pena, [illegible]erez, M., Clare, J., Asher, G., Wheeler, [illegible] "Power S[illegible] Using a Flywheel Driven by a Switched Reluctance Mach[illegible]e", IEEE Transactions on Industrial Electronics, [illegible]–1093, 2006. https://doi.org/10.1109/TIE.2006.878325

[10] Beniwal, J. L., Tripathi, R. K. "A novel four-phase active boost switched reluctance inverter for high speed SRM drive", International Journal of Power Electronics and Drive Systems (IJPEDS), 8(4), pp. 1562–1574, 2017. https://doi.org/10.11591/ijpeds.v8.i4.pp1562-1574

[11] Mekala, N., Muniraj, C. "Implementation of PI Controller for 4ϕ Srm Drive Using TMS320F28335", International Journal of Power Electronics and Drive System (IJPEDS), 5(3), pp. 283–292, 2017. https://doi.org/10.11591/ijpeds.v5.i3.pp283-292

[12] Barros, T. A. D. S., Neto, P. J. D. S., Filho, P. S. N., Moreira, A. B., Filho, E. R. "An approach for switched reluctance generator in awind generation system with a wide range of operation speed", IEEE Transactions on Power Electronics, 32(11), [illegible]2, 2017. https://doi.org/10.1109/TPEL.2017.2697822

[13] Viajante, G. P., Chaves, E. N., Queiroz, C. [illegible]reitas, M. A. A., Miranda, L. C., Silva, D. P. A., Silv[illegible] B., Gom[illegible]. C., Fidelis, L. T. "A grid connection scheme [illegible] switched relucta[illegible] generat[illegible] using P+Resonant controlle[illegible]n: Conferen[illegible] Proceed[illegible]7 IEEE International Con[illegible]ce on En[illegible]ment and Electrical Engineering and 20[illegible] IEEE [illegible]ust[illegible] and Comme[illegible]ial Power Systems Europe ([illegible]EIC / I and [illegible] Europe), M[illegible], Italy, 2017, pp. 1–6. ISBN [illegible]1-5386-3918-4 https://doi[illegible]10.[illegible]/EEEIC.2017.797[illegible]

[14] Besmi, M. "Geomet[illegible] Design of Switched Reluctance Motor to Reduce the Torque [illegible]le by Finite Element Method and [illegible] Analysis", Journ[illegible]f Electric Power and Energy Conversion Systems (JEPECS), 1(1), pp. 23–31, 2013. [online] Available at: https://research.shahed.ac.ir/WSR/SiteData/PaperFiles/8532_[illegible]956392.pdf [Accessed: 20 December 2022]

[1[illegible]] Teixeira, V., Oli[illegible]a, D., Pontes, R., Viana, S. "Influence of the [illegible]tched reluc[illegible]e machines design parameters on its steady-state ope[illegible]aracteristics", In: 2007 International Conference on Electrical Machines and Systems (ICEMS), Seoul, South-Korea, [illegible] pp. 1455–1459. https://doi.org/10.1109/ICEMS12746.2007.4412081

[16] Somesan, L., Padurariu, E., Viorel, I. "Two Simple Analytical Models, Direct and Inverse, for Switched Reluctance Motors", Progress in Electromagnetics Research M, 29, pp. 279–291, 2013. https://doi.org/10.2528/PIERM12103001

[17] Ma, C., Qu, L. "Multiobjective optimization of switched reluctance motors based on design of experiments and particle swarm optimization", IEEE Transactions on Energy Conversion, 30(3), pp. 1144–1153, 2015. https://doi.org/10.1109/TEC.2015.2411677

[18] Tang, Y. "Characterization, numerical analysis, and design of switched reluctance motors", IEEE Transactions on Industry Applications, 33(6), pp. 1544–1552, 1997. https://doi.org/10.1109/28.649967

[19] Mousavi-Aghdam, S. R., Feyzi, M. R., Ebrahimi, Y. "A New Switched Reluctance Motor Design to Reduce Torque Ripple using Finite Element Fuzzy Optimization", Iranian Journal of Electrical and Electronic Engineering, 8(1), pp. 91–96, 2012. [online] Available at: http://ijeee.iust.ac.ir/article-1-373-en.html [Accessed: 20 December 2022]

[20] Raminosoa, T., Blunier, B., Fodorean, D., Miraoui, A. "Design and Optimization of a Switched Reluctance Motor Driving a Compressor for a PEM Fuel-cell System for Automotive Applications", IEEE Transactions on Industrial Electronics, 57(9), pp. 2988–2997, 2010. https://doi.org/10.1109/TIE.2010.2041133

[21] JaymeDias, R., Reategui Silva, C., Reis dos Santos, B., dos Santos Costa, C., Fleury Veloso da Silveira, A., Alves de Andrade, D. "Innovations on Design of 6x4 and 6x6 Switched Reluctance Generators for Increasing the Efficiency", IEEE Latin America Transactions, 15(4), pp. 646–655, 2017. https://doi.org/10.1109/TLA.2017.7896350

[22] Cheng, H., Chen, H., Yang, Z. "Design indicators and structure optimisation of switched reluctance machine for electric vehicles", IET Electric Power Applications, 9(4), pp. 319–331, 2015. https://doi.org/10.1049/iet-epa.2014.0291

[23] Bajec, P., Zidaric, B., Miljavec, D. "Artificial Neural Network Modeling of Synchronous Reluctance Motor", In: Progress In Electromagnetics Research Symposium, Marrakesh, Morocco, 2011, pp. 1854–1858. ISBN 9781934142165

[24] Mao, S. H., Tsai, M. C. "A novel switched reluctance motor with C-core stators", IEEE Transactions Magnetics, 41(12), pp. 4413–4420, 2005. https://doi.org/10.1109/TMAG.2005.858372

[25] Vijayraghavan, P. "Design of Switched Reluctance Motors and Development of a Universal Controller for Switched Reluctance and Permanent Magnet Brushless DC Motor Drives", PhD Thesis, Virginia Polytechnic Institute and State University, 2001. [online] Available at: http://hdl.handle.net/10919/29799 [Accessed: 20 December 2022]

[26] Krishnan, R. "Switched Reluctance Motor Drives", Taylor & Francis Inc., 2001. ISBN 9780849308383

[27] Choi, Y. K., Yoon, H. S., Koh, C. S. "Poleshape optimization of a switched-reluctance motor for torque ripple reduction", IEEE Transactions on Magnetics, 43(4), pp. 1797–1800, 200[illegible] https://doi.org/10.1109/TMAG.2006.892292

[28] Gan, C., Wu, J., Sun, Q., Kong, W., Li, H., H[illegible]. "A review on machine topologies and control techniques for lo[illegible]ise switched reluctance motors in electric vehicle a[illegible]cations", [illegible]E Access, 6, pp. 31430–31443, 2018. https://doi.org/10.1109/ACCESS[illegible]8.2837111

[29] Lee, J. W., Kim, H. S., Kwo[illegible] I., Kim, [illegible] "New rotor sh[illegible]e design for minimum to[illegible]ue rip[illegible] of [illegible]M using FEM[illegible] IEEE Transactions on Mag[illegible]cs, 40(2), p[illegible]4–757, 2004 https://doi.org/10[illegible]/TMAG.2004.824[illegible]

[30] Di Barbaa, [illegible]vell[illegible]Mognaschi, M., P[illegible]ski, M., Rezaei, N., Slusarek B., Wiak, [illegible]Geometry optimization for a class of switched-reluctance motors[illegible] bi-objective approach", Interna-ti[illegible]l of Applied Electro[illegible]netics and Mechanics, 56(S1), [illegible]. 107–122, 2018. [illegible]ttps://doi.org/10.3[illegible]JAE-172282